Diamond & Related Materials 65 (2016) 183–190

Contents lists available at ScienceDirect

Diamond & Related Materials

journal homepage: www.elsevier.com/locate/diamond

Hybrid gas sensor based on platinum nanoparticles/poly(methyl methacrylate)-coated single-walled carbon nanotubes for dichloromethane detection with a high response magnitude

Worawut Muangrat [a], Visittapong Yordsri [b], Rungroj Maolanon [c], Sirapat Pratontep [a,d,e], Supanit Porntheeraphat [f], Winadda Wongwiriyapan [a,d,e,*]

[a] College of Nanotechnology, King Mongkut's Institute of Technology Ladkrabang, Chalongkrung Rd., Ladkrabang, Bangkok 10520, Thailand
[b] National Metal and Materials Technology Center, Phahonyothin Rd., Khlong Luang, Pathumthani 12120, Thailand
[c] National Nanotechnology Center, Phahonyothin Rd., Khlong Luang, Pathumthani 12120, Thailand
[d] Nanotec-KMITL Center of Excellence on Nanoelectronic Devices, Chalongkrung Rd., Ladkrabang, Bangkok 10520, Thailand
[e] Thailand Center of Excellence in Physics, CHE, 328 Si Ayutthaya Rd., Bangkok 10400, Thailand
[f] National Electronics and Computer Technology Center, Phahonyothin Rd., Khlong Luang, Pathumthani 12120, Thailand

ARTICLE INFO

Article history:
Received 1 December 2015
Received in revised form 15 March 2016
Accepted 17 March 2016
Available online 24 March 2016

Keywords:
Single-walled carbon nanotube
Dichloromethane
Poly(methyl methacrylate)
Platinum nanoparticles
Gas sensor

ABSTRACT

A dichloromethane (DCM) sensor with a high response magnitude was successfully fabricated using the integration of single-walled carbon nanotubes (SWNTs), poly(methyl methacrylate) (PMMA) and platinum nanoparticles (Pt NPs). A pristine SWNT network was first formed by drop-casting onto printed circuit board (PCB) substrates. Next, PMMA was coated onto the pre-dropped SWNT network by spin coating using a PMMA-toluene solution, followed by the deposition of Pt NPs by electron-beam evaporation (hereafter referred to as Pt/PMMA/SWNT). The Pt/PMMA/SWNT enabled an approximately 69-fold improvement in DCM detection compared to pristine SWNT. The high response magnitude of the Pt/PMMA/SWNT was successfully achieved because of the incorporation of PMMA and Pt functions. Swelling of the PMMA matrix as a result of DCM adsorption leads to PMMA volume expansion, thereby increasing the SWNT-SWNT distance, which results in an increase in the resistance. Pt NPs promote the dissociation of DCM to CO, and consequently the CO oxidation on the Pt NPs catalyst and electron donation from Pt NPs to SWNTs, resulting in an increase in the resistance. Moreover, a linear relationship was obtained between the sensor response of the Pt/PMMA/SWNT and the concentration of DCM. These results suggest that the integration of SWNTs with PMMA and Pt NPs is a promising approach for improving DCM detection at room temperature.

1. Introduction

Volatile organic compounds (VOCs) [1] have been widely used in various industrial processes and commercial products, such as transport, household chemicals, paints and adhesives. Several VOCs are directly harmful to environmental and human health even at trace levels in ambient air. For example, dichloromethane (DCM, CH_2Cl_2), which is mainly used in the metal surface degreasing and electronics industry, is known as the cause of respiratory and central nervous system, chronic toxicity and carcinogenicity [2–4]. Hence, environmental monitoring and industrial safety are absolutely crucial for the protection of environmental and human health. Since the last decade, the most widely used analytical methods for VOC detection have been gas chromatography/mass spectrometry (GC/MS), high-performance liquid chromatography (HPLC) and photoionization detection (PID) because of their high sensitivity and reliability. Nevertheless, their practical application is highly limited as a result of their complexity, relatively high cost, unportability and calibration requirements to maintain accuracy. Recently, a gas sensor based on the simple change in its resistance in response to analytes has become a promising candidate for practical sensing devices. The advantages of a gas sensor include its compact size, real-time monitoring and low power consumption. Gas sensors based on metal oxide materials have been widely developed for VOC detection with a detection limit down to the parts per million (ppm) level [5,6]. Despite their high sensitivity, these sensors exhibit drawbacks, including nonselectivity and high power consumption (operating temperature > 200 °C). Several nanostructured materials, such as single-walled carbon nanotubes (SWNTs) [7], have attracted considerable attention as alternative sensing materials because of their distinctive characteristics in structural, electrical, optical, mechanical and thermal properties. SWNTs have shown outstanding potential for gas sensing

---

[*] Corresponding author at: College of Nanotechnology, King Mongkut's Institute of Technology Ladkrabang, Chalongkrung Rd., Ladkrabang, Bangkok 10520, Thailand.
E-mail address: winadda.wo@kmitl.ac.th (W. Wongwiriyapan).

http://dx.doi.org/10.1016/j.diamond.2016.03.016
0925-9635/

applications because of their well-organized nanostructure, large specific surface area [8] and electrical properties [9,10]. SWNT-based sensors have demonstrated high response to oxidizing gases down to the parts per billion (ppb) level under room-temperature operation [11–14]; however, they are weakly sensitive to VOCs. In recent years, to overcome these obstacles, many efforts have been made aiming to improve the VOC sensing performance of such sensors by means of SWNTs functionalized with polymers [15–18] and metal nanoparticles (NPs) [19–21]. For instance, a gas sensor based on functionalized-multi-walled carbon nanotubes and poly(methyl methacrylate) composites (f-MWNT-PMMA) by dip-coating technique has been demonstrated for VOC detection [15,16]. This f-MWNT-PMMA-based sensor shows a high response to a saturated vapor of DCM [15] but a low sensor response to DCM vapor in a partial pressure range of 27–273 Torr [16]. In addition, MWNTs were functionalized using potassium permanganate with the help of a phase transfer catalyst. Although the major advantage of this process is a high yield of functionalized MWNTs, but it is time-consuming and involves the use of hazardous chemicals. Another type of gas sensor was fabricated using conductive polymer-MWNT composites by spray layer by layer (sLbL) without further treatment of MWNTs for VOC detection at a saturated vapor [17]. Recently, W. Muangrat et al. [18] demonstrated a simple preparation of gas sensor by spin-coating PMMA on the drop-casted SWNTs (PMMA/SWNT). The sensor response of PMMA/SWNT to DCM greatly increases 5.4-fold higher than that of pristine SWNTs. The sensing mechanism of the polymer-functionalized carbon nanotubes (CNTs) is attributed to the swelling of the polymer matrix upon exposure to the organic vapor molecules, leading to volume expansion, and thereby giving rise to an increase in the CNT–CNT distance, resulting in an increase in the resistance. Additionally, the deposition of palladium (Pd) and platinum (Pt) nanoparticles (NPs) on MWNTs enhances the sensor response toward aromatic VOCs (benzene and toluene) and non-aromatic VOCs (acetone, ethanol and methanol) [21]. The sensing mechanism of metal NP-decorated CNTs can be explained by the electron transport from the metal NPs to the CNTs, resulting in an increase in the resistance. As mentioned above, polymer and metal NPs are effective in improving VOC sensitivity by different mechanisms. Thus, utilizing the functions of both the polymer and the metal NPs in a single device is a promising route to improving its VOC sensitivity and response magnitude.

In this work, we successfully demonstrated highly sensitive detection of DCM vapor under room temperature conditions by means of SWNTs functionalized with PMMA and Pt NPs without further SWNT treatment. The response magnitude of the hybrid sensor to DCM was 69-fold higher than that of pristine SWNTs and linearly increased with increasing DCM concentration. The sensing mechanism was elucidated by catalytic oxidation on the Pt NPs catalyst surface and polymer swelling. The proposed hybrid sensor shows figures of merit over the previous reports in terms of the simplicity in sensor fabrication and the enhancement of the sensor response magnitude to VOCs at the concentration lower than a saturated vapor.

2. Experimental methods

2.1. Fabrication of gas sensor device

A printed circuit board (PCB) consisting of an interdigitated Cu/Au electrode with a gap of 250 μm was used as the sensor platform. An SWNT suspension was prepared by dispersing SWNTs, (diameter and length in the ranges of 1.2–1.5 nm and 2–5 μm, respectively) in 1,2-dichloroethane by ultrasonication for 3 h and subsequently dropping onto the PCB. The electrical resistance of the SWNT on the PCB was adjusted to approximately 100 kΩ. A solution of PMMA ($M_w = 94{,}600$ g/mol) was prepared in toluene and stirred for 24 h. Then, the PMMA solution was spin-coated onto the predropped SWNT network at a spinning speed of 3000 rounds per minute for 5 min, followed by heating at 100 °C for 24 h to eliminate the solvent in the sensor samples. The PMMA concentration was varied between 1 and 5 wt.%. Next, the prepared PMMA-coated SWNTs were deposited with Pt NPs by electron-beam evaporation. The amount of the deposited Pt NPs was monitored by a quartz crystal oscillator embedded in the electron-beam evaporation equipment as a thickness of 2 and 5 nm (hereafter referred to as Pt/PMMA/SWNT). For comparison, SWNTs with only a PMMA coating or Pt NP decoration were also fabricated (hereafter referred to as PMMA/SWNT and Pt/SWNT, respectively). A schematic view of the hybrid sensor and details of the fabricated gas sensor are shown in Fig. 1 and Table 1, respectively.

2.2. Characterization techniques

The morphologies of the pristine SWNTs and PMMA/SWNTs were characterized by field emission scanning electron microscopy (FESEM; JEOL JSM-7800F). The FESEM observation was carried out in a high vacuum mode with a base pressure of approximately 9×10^{-5} Pa and an acceleration voltage of 1 kV without any surface treatment with metallic materials. The elemental composition of Pt/PMMA/SWNT was studied by FESEM equipped with an energy dispersive X-ray spectrometer (EDS; OXFORD). Transmission electron microscopy (TEM; JEOL JE-2010) was employed to characterize the nanostructure of the Pt/SWNTs. The carbon structure, purity and crystallinity were analyzed by Raman spectroscopy (Thermo SCIENTIFIC DXR) with an Ar ion laser wavelength of 532 nm (2.33 eV). The crystal structure was characterized by X-ray diffraction (XRD; Rigaku TTRAX II) using Cu Kα with a wavelength of 1.54 Å at a scan rate of 1 °/min. The functional group of PMMA was characterized by Fourier transform infrared spectroscopy (FTIR; Perkin Elmer, Spectrum One). The FTIR sample was prepared by mixing SWNTs powder with potassium bromide (KBr) and pressing in a pellet form. Then, the prepared pellet was coated and decorated with PMMA and Pt NPs, respectively. Typical FTIR spectra in an absorbance mode were scanned in a wavenumber range of 500–4000 cm^{-1}.

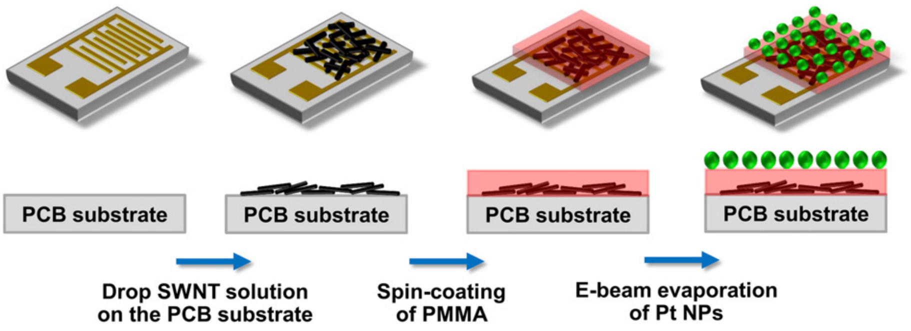

Fig. 1. Schematic view of hybrid sensor.

Table 1
Summary of sensors based on hybrid SWNTs.

Sensor configuration	Designation of sensor
Pristine SWNT	$S_{0,0}$
PMMA(1 wt.%)/SWNT	$S_{0,1}$
PMMA(5 wt.%)/SWNT	$S_{0,5}$
Pt(2 nm)/SWNT	$S_{2,0}$
Pt(5 nm)/SWNT	$S_{5,0}$
Pt(2 nm)/PMMA(1 wt.%)SWNT	$S_{2,1}$
Pt(2 nm)/PMMA(5 wt.%)SWNT	$S_{2,5}$
Pt(5 nm)/PMMA(1 wt.%)SWNT	$S_{5,1}$
Pt(5 nm)/PMMA(5 wt.%)SWNT	$S_{5,5}$

2.3. Gas sensor measurement

The sensor response to DCM vapor was investigated at room temperature by recording the electrical resistance using a FLUKE NetDAQ during cycles of alternating supply of dry N_2 gas and DCM vapor. The sensors were placed in a stainless steel chamber and N_2 gas was introduced into the chamber at a flow rate of 3.0 lpm for 600 s as a baseline. Then, N_2 was replaced with DCM vapor by bubbling liquid DCM with N_2 carrier gas at a flow rate of 1.5 lpm for 300 s. The concentration of the DCM vapor was adjusted by controlling the temperature of the DCM liquid. The sensors were recovered by purging with 3.0 lpm of N_2 for 600 s. The sensor response (SR) was defined as $SR = (R_{DCM} - R_0) / R_0$, where R_{DCM} and R_0 are the resistances of the sensor after and before DCM exposure, respectively. To compare the responses of all the sensors, the sensor responses were normalized by the DCM concentration. The normalized sensor response (NSR) was defined as the ratio between the sensor response at a time of 900 s (SR_{900}) and the DCM concentration (C_{DCM}): $NSR = SR_{900} / C_{DCM}$.

3. Results and discussion

3.1. Characterization of sensor materials: morphology, structure, composition, and crystallinity

First, pristine SWNTs and PMMA/SWNTs were morphologically characterized by FESEM. The pristine SWNTs assembled into a network of overlying SWNTs, forming a conductive network structure on the substrate, as shown in Fig. 2(a). Fig. 2(b and c)shows the cross-sectional FESEM images of PMMA(1 wt.%)/SWNT ($S_{0,1}$) and PMMA(5 wt.%)/SWNT ($S_{0,5}$), respectively. The thicknesses of the PMMA(1 wt.%) and PMMA(5 wt.%) coatings on the SWNTs were 0.40 and 2.64 μm, respectively. From the FESEM image of $S_{0,1}$ (Fig. 2(b)), the SWNT network was shown to be buried in the PMMA matrix and some of the SWNT bundles were protruding from the PMMA surface. However, in the case of $S_{0,5}$, PMMA(5 wt.%)/SWNT, PMMA completely covered the pristine SWNT network. The thickness of the PMMA film was controlled by the concentration and viscosity of the PMMA solution. Fig. 1(d and e)shows the TEM images of the Pt-decorated SWNT with different Pt loading amounts ($S_{2,0}$ and $S_{5,0}$, respectively). The Pt NPs were attached to the sidewalls of the pristine SWNT bundles, whereas the SWNT bundles maintained their structure. The average diameters of the Pt NPs of $S_{2,0}$ and $S_{5,0}$ were 3.53 ± 0.94 and 4.04 ± 0.77 nm, respectively. The Pt NPs on $S_{5,0}$ exhibited greater coverage and a narrower size distribution compared to those of $S_{2,0}$. For Pt/PMMA/SWNT, it is hard to directly observe its structure by TEM because of the damage of the electron beam on PMMA. Thus, FESEM-EDS, XRD and FTIR techniques were utilized to confirm the existence of the Pt NPs and PMMA in the Pt/PMMA/SWNT.

The elemental composition of $S_{5,5}$ was determined by EDS. The analyzed surface area for EDS mapping is shown in Fig. 3(a). The EDS elemental mapping image revealed that $S_{5,5}$ consists of Pt (in purple), carbon (in red) and oxygen (in green), as shown in Fig. 3(b–d), respectively. The Pt mapping clearly indicates that the Pt NPs are homogeneously distributed on the $S_{5,5}$ as shown in Fig. 3(b). Carbon and

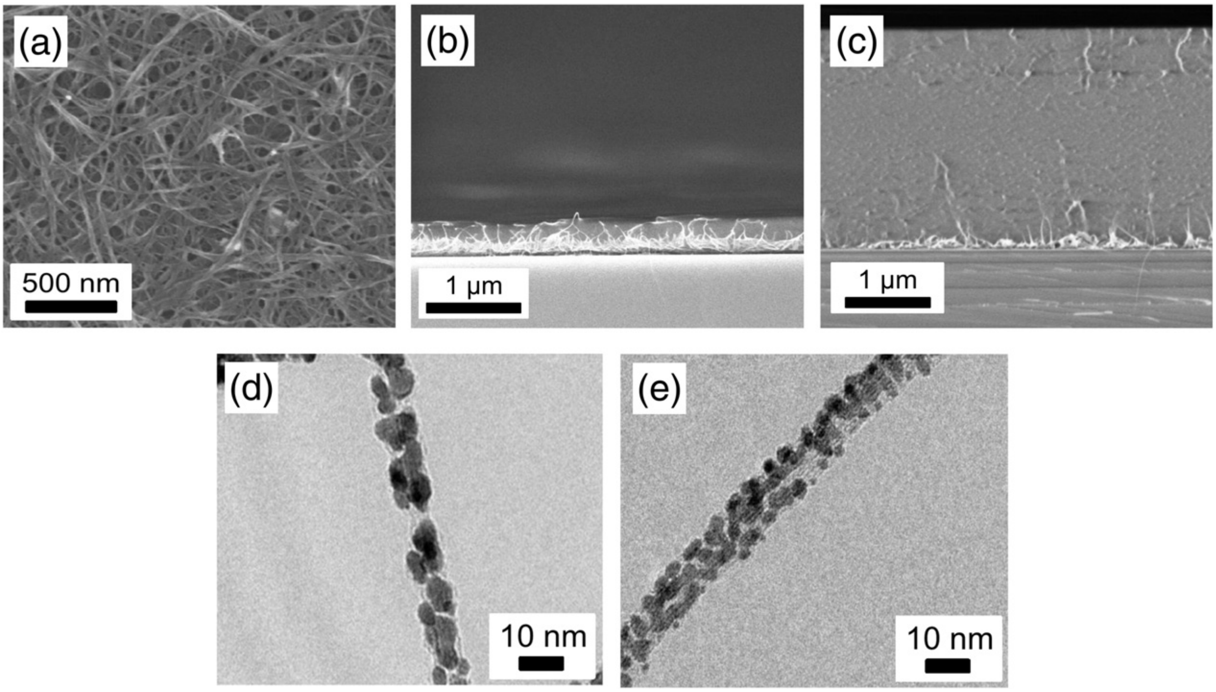

Fig. 2. FESEM images of (a) $S_{0,0}$, (b) $S_{0,1}$, and (c) $S_{0,5}$. TEM images of (d) $S_{2,0}$ and (e) $S_{5,0}$.

oxygen elements may be derived from SWNT and PMMA. To confirm the PMMA existence in the $S_{5,5}$, the sample was characterized by FTIR. Fig. 3(e) shows FTIR spectra of $S_{0,0}$, $S_{0,5}$ and $S_{5,5}$. FTIR spectra of $S_{0,5}$ and $S_{5,5}$ show almost identical feature. The peak assigned to the C–H stretching vibration occurred at 2977 cm^{-1}. The strong peak at 1730 cm^{-1} is assigned to C=O stretching vibration. The peaks at 1157, 1199, and 1265 cm^{-1} correspond to C–O–C stretching and deformation vibrations. The peaks observed at 999 cm^{-1} and 858 cm^{-1} are due to C–H bending vibrations and the peak at 746 cm^{-1} is attributed to the vibrations of the polymer chains [22,23]. This result confirms the existence of PMMA and the same composition of the functional group of PMMA before and after Pt deposition.

To confirm the crystallinity, the sample was characterized by XRD. The typical XRD diffraction patterns of $S_{0,5}$, $S_{5,0}$ and $S_{5,5}$ are shown in Fig. 3(f). $S_{0,5}$ exhibited a broad peak at ~13°, which corresponds to the structure of PMMA [24], whereas the diffraction peaks of $S_{5,0}$ located at 39.7° and 46.2° can be assigned to reflections from the (111) and (200) planes of the face-centered cubic Pt, respectively [25,26]. The (111) and (200) diffraction peaks of the Pt NPs at $2\theta = 39.7°$ and 46.2° correspond to d-spacings of 0.227 and 0.196 nm, respectively. For $S_{5,5}$, the XRD diffraction pattern shows a diffraction peak from PMMA at ~13° and diffraction peaks from Pt NPs at 39.7° and 46.2°, respectively, confirming the existence of PMMA and Pt NPs. However, $S_{5,5}$ has a slightly broader peak from PMMA at ~13°, indicating the higher weight fraction of amorphous PMMA after Pt deposition. These results imply changes in the structural regularity of the main chains of the polymeric molecules. The average size of the Pt NPs was calculated from the Pt(111) peak using the Scherrer equation: $L = (0.9\lambda_{K\alpha}) / \beta_{(2\theta)}\cos\theta$, where L is the mean size of the Pt NPs, λ is the X-ray wavelength (Cu $K\alpha = 1.54$ Å), θ is half of the scattering angle, and β is the full-width half-maximum (FWHM) of the X-ray diffraction [25]. The calculated Pt NPs average sizes of $S_{5,0}$ and $S_{5,5}$ were approximately 3.99 and 3.29 nm, respectively, which are consistent with the TEM results.

Raman spectroscopy was utilized to characterize the structure, purity and crystallinity of SWNT. Fig. 4(a) shows the four significant Raman peaks: SWNT-derived Raman breathing mode (RBM) at 190

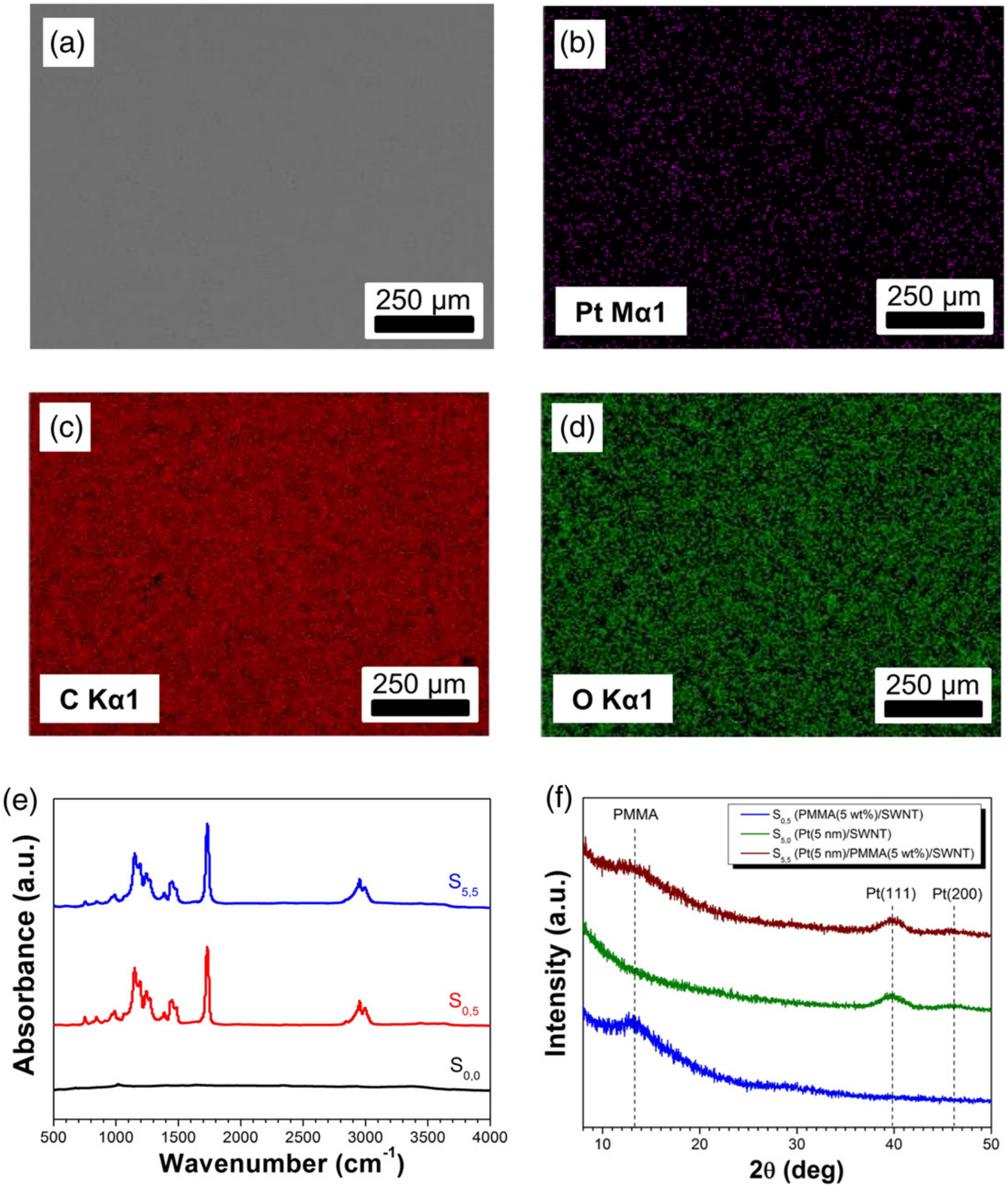

Fig. 3. (a) FESEM images of $S_{5,5}$ and EDS-mapping of (b) platinum, (c) carbon, and (d) oxygen elements. (e) FTIR spectra of $S_{0,0}$, $S_{0,5}$, and $S_{5,5}$. (f) XRD spectra of $S_{0,5}$, $S_{5,0}$, and $S_{5,5}$.

and 273 cm^{-1}, disorder carbon-derived D-band at 1332 cm^{-1} and graphitic-structure-derived G-band at 1588 cm^{-1}. The intensity ratio between the G- and D-bands (I_G/I_D) of pristine SWNTs was approximately 14.03 ± 1.2. After PMMA coating, the I_G/I_D ratios of $S_{0,1}$ and $S_{0.5}$ were 14.32 ± 0.8 and 14.79 ± 2.1, respectively, with no obvious difference from the pristine SWNTs. However, after Pt decoration, the I_G/I_D ratio of $S_{2,0}$ and $S_{5.0}$ were significantly decreased to 9.38 ± 0.3 and 3.99 ± 0.7, respectively, implying that the crystallinity and purity of the SWNTs deteriorated, especially for $S_{5,0}$ in which the highest amount of Pt NPs showed the lowest I_G/I_D value. The decrease in the I_G/I_D value could be attributed to the damage during Pt NPs adhesion on the SWNTs with high energy. For Pt/PMMA/SWNT, the I_G/I_D values of $S_{2,1}$, $S_{5,1}$, $S_{2,5}$, and $S_{5.5}$ were 13.32 ± 0.8, 5.62 ± 0.7, 13.37 ± 0.9 and 11.36 ± 0.6, respectively. The I_G/I_D values of $S_{2,5}$ and $S_{5,5}$ were greater than those of $S_{2,0}$, $S_{5.0}$ $S_{2,1}$ and $S_{5,1}$, indicating higher crystallinity and purity of the SWNTs. These results show that a thick film of PMMA effectively protects the SWNTs during Pt NPs deposition. Fig. 4(b) shows RBM spectra derived from $S_{0,0}$, $S_{2,0}$, $S_{5,0}$ and $S_{5,5}$. The diameter of the pristine SWNTs (d) can be estimated from the RBM peak using the formula $d = 248/\Omega_{RBM}$ [27], where Ω_{RBM} is the Raman shift of RBM peak. Although SWNTs with d ≥ 2 nm are generally difficult to detect by Raman spectroscopy, this laser excitation shows the existence of SWNTs with diameters of 0.91 and 1.31 nm. The intensity of the RBM peak at 273 cm^{-1} and the I_G/I_D ratios of $S_{2,0}$ and $S_{5,0}$ gradually decreased with increasing amount of deposited Pt NPs on the pristine SWNT, whereas those of $S_{5,5}$ were relatively comparable to those of the pristine SWNTs. The decrease in the RBM peak and I_G/I_D ratios of $S_{2,0}$ and $S_{5,0}$ is attributed to the damage of small-diameter SWNTs during Pt NPs adhesion with high energy. These results also clearly confirm that PMMA can act as a protective layer on SWNTs during Pt NP deposition.

3.2. Gas sensing characteristics

Fig. 5(a and b)shows sensor responses as a function of time of each sensor under an alternating supply of DCM (1700 mg/L) and N_2 gas for 5 cycles. Fig. 5(c) shows the normalized sensor response of each sensor to DCM. The electrical resistance of all the sensors increased upon DCM exposure and decreased after replacing DCM with N_2 gas (Fig. 5(a and b)). $S_{0,0}$, $S_{0,1}$, and $S_{0,5}$, were recovered to their initial resistances by N_2 gas purging. Conversely, $S_{2,0}$ and $S_{5,0}$ were hardly recovered to their initial resistances. The different response characteristics between PMMA/SWNT and Pt/SWNT may be attributed to the difference in DCM molecule adsorption behaviors. In the case of $S_{0,0}$, $S_{0,1}$, and $S_{0,5}$, DCM molecules are likely to physically adsorb onto the pristine SWNTs and the PMMA/SWNTs via van der Waals forces, which is a weak interaction. Thus, DCM molecule was easily removed by N_2 gas purging. In the case of $S_{2,0}$ and $S_{5,0}$, DCM molecules seem to strongly interact with the Pt NPs through chemisorption, which is relatively stronger interaction than the physisorption, resulting in difficulty in removing DCM molecule from sensor material, especially in the case of $S_{5,0}$. The Pt/PMMA/SWNT also shows the similar recovery behavior to the Pt/SWNT. The reversibility of the sensor can be improved by applying heat or UV exposure, similar to SWNT sensor system [12–14]. Regarding the response time of the sensor, the response time is defined as the time taken by the sensor to reach 90% of its maximum sensor response. The pristine SWNT showed the fastest response with a response time of approximately 17 ± 4 s, but it exhibited the smallest response magnitude. On the other hand, the hybrid Pt/PMMA/SWNT enabled 69-fold improvement in DCM detection compared to the pristine SWNT. However, the response time of the Pt/PMMA/SWNT increased up to 190 ± 6 s, which is approximately 11-time higher than that of the pristine SWNT. The hybrid Pt/PMMA/SWNT shows a merit for a significant enhancement of sensor response magnitude but there is room for improvement in its response time.

The sensing mechanism of the pristine SWNTs can be described in terms of the dielectric constant, which involves the solvent polarity of DCM. Molecules with polarity can hold moving holes and interrupt movement of holes along the p-type SWNTs, resulting in an increase in electrical resistance and thus an increase in sensor response [28]. The sensor responses of $S_{0,1}$, and $S_{0,5}$ toward DCM greatly increased 8.0- and 14.9-fold compared to that of $S_{0,0}$ (Fig. 5(c)), indicating sensor response enhancement by PMMA functionalization. The sensing mechanism could be explained by polymer swelling as a result of DCM adsorption. A hypothesis based on polymer swelling can be described as follows: after DCM adsorption, the PMMA coating on the SWNTs swell, possibly increasing the PMMA volume and loosening the SWNT network in the polymer [15,16,18], which would result in an increase in the electrical resistance. Furthermore, $S_{0,5}$ shows a higher response to DCM compare to $S_{0,1}$. These results may be attributed to the effect of the PMMA film thickness coating on the SWNTs (Fig. 2(b and c)). A thicker film enhances swelling, resulting in a higher sensor response.

For Pt/SWNTs, the sensor response of $S_{2,0}$ and $S_{5,0}$ to DCM greatly increased 2.7- and 21.4-fold higher than that of $S_{0,0}$ (Fig. 5(c)), indicating sensor response improvement by Pt NP functionalization. We envision that the sensing mechanism of Pt/SWNT toward DCM is similar to that of Pt-deposited SWNTs toward CO systems [29]. The mechanism is based on the dissociation of DCM to CO and subsequently CO oxidation on the Pt catalyst surface. The surface of the Pt NPs is saturated with chemisorbed O_2 molecules under atmospheric pressure [30], whereas some O_2 molecules are dissociated into O^- on the surface of Pt NPs. Upon exposure to DCM, DCM molecule reacts with the pre-adsorbed O_2 and dissociate on the Pt NP surface according to the reaction

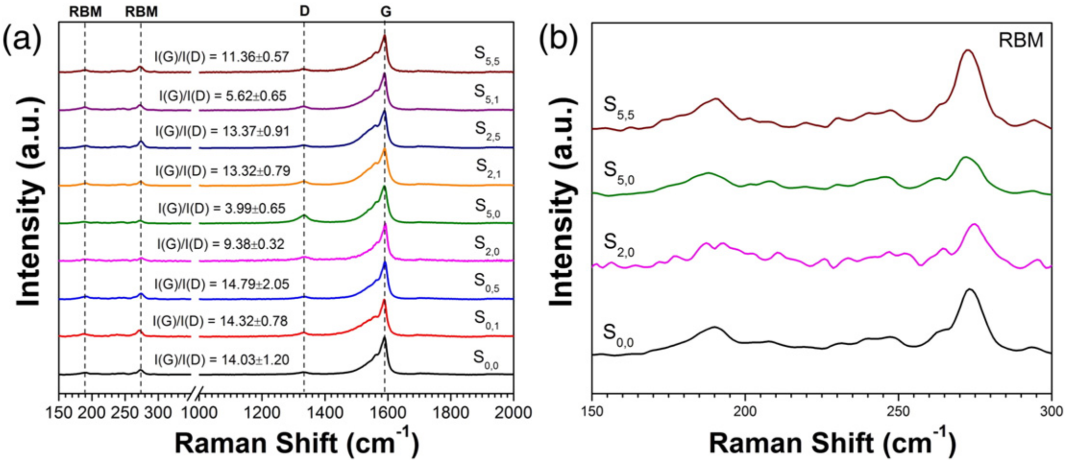

Fig. 4. (a) Raman spectra of all sensors and (b) RBM spectra of $S_{0,0}$, $S_{2,0}$, $S_{5,0}$, and $S_{5,5}$.

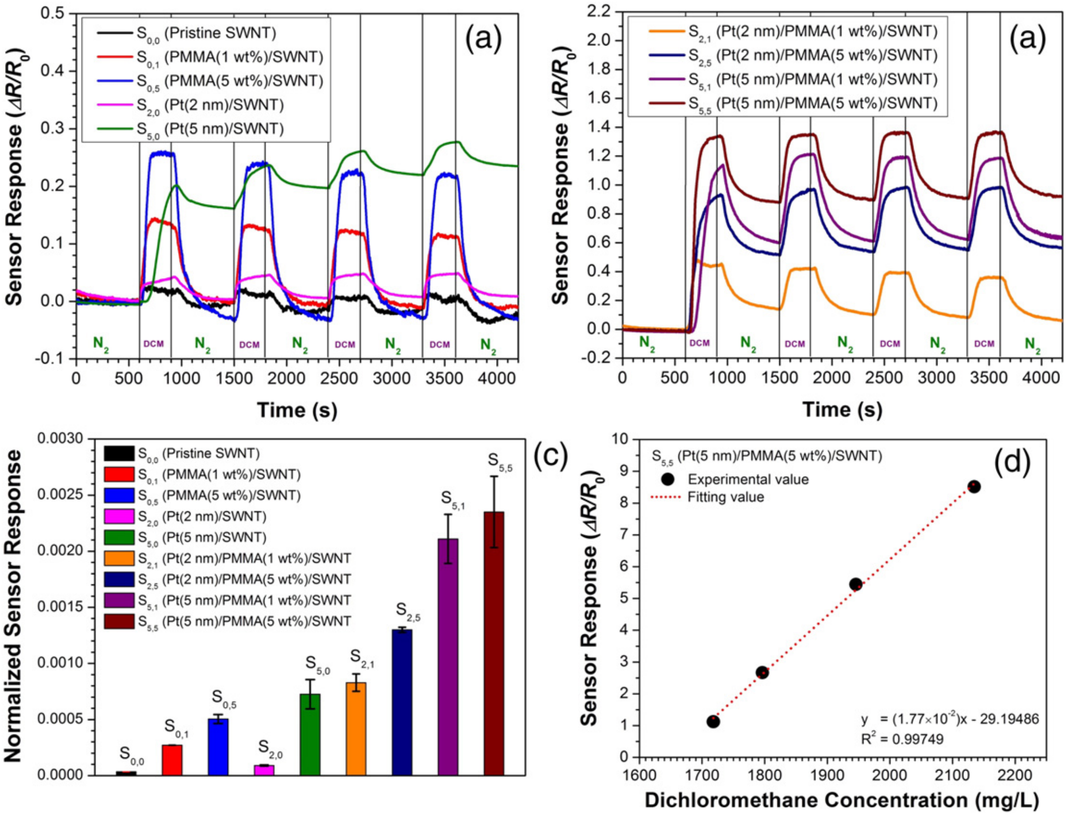

Fig. 5. Sensor response as a function of time for (a) $S_{0,0}$, $S_{0,1}$, $S_{0,5}$, $S_{2,0}$, and $S_{5,0}$ and (b) $S_{2,1}$, $S_{2,5}$, $S_{5,1}$, and $S_{5,5}$ toward DCM vapor; (c) normalized sensor response of all sensors toward DCM; and (d) sensor response of $S_{5,5}$ as a function of DCM concentration.

$CH_2Cl_2(g) + (1/2)O_2(ad) \rightarrow CO(g) + 2HCl(g)$ [31]. Consequently, CO interacts with O^- by the reaction, $CO(ad) + O^-(ad) \rightarrow CO_2(g) + e^-$, via the Langmuir–Hinshelwood mechanism [29,32]. Finally, the electron captured by pre-adsorbed O^- is released and donated to the p-type semiconducting SWNT, resulting in an increase in electrical resistance. $S_{5,0}$ shows higher response to DCM than does sensor $S_{2,0}$. A uniform size distribution, full coverage and nanometer-sized Pt NPs on the SWNTs of $S_{5,0,}$ as confirmed by the TEM images in Fig. 2(d and e), result in the high sensitivity of $S_{5,0}$ to DCM.

For the integration sensors of SWNTs, PMMA and Pt NPs ($S_{2,1}$, $S_{2,5}$, $S_{5,1}$ and $S_{5,5}$), all of the sensors selectively responded to DCM vapor with high response magnitude. In particular, the sensor response of $S_{5,5}$ toward DCM greatly increased by 69.4-fold compared to that of $S_{0,0}$. The high response magnitude of the Pt/PMMA/SWNTs was successfully achieved as a result of the incorporation of PMMA and Pt functions. The sensing mechanism of the Pt/PMMA/SWNTs could possibly explain by the combination of the following phenomena, which involve catalytic oxidation on the Pt surface and polymer swelling. Regarding the catalytic reaction on the Pt surface of the Pt/PMMA/SWNT based on PMMA 1 wt.% ($S_{2,1}$ and $S_{5,1}$), the thickness of the PMMA layer was approximately 0.40 μm. SWNT network was partly buried in the PMMA matrix and some of the SWNT bundles were clearly seen to protrude from the PMMA surface (Fig. 2(b)). Thus, the released electron from dissociation reaction of DCM can directly donate to the SWNTs. In the case of the Pt/PMMA/SWNT based on PMMA 5 wt.%, the thickness of the PMMA layer was approximately 2.64 μm ($S_{2,5}$ and $S_{5,5}$). PMMA completely covered the pristine SWNT network. However, a careful observation of Fig. 2(c) reveals that there are bundles of SWNTs were drawn to the surface of the PMMA layer, forming a conduction path in the SWNT-PMMA matrix, as shown in Fig. 2(c) as a white line. Thus, these SWNT bundles can act as a conductive path for the released electron through the PMMA to the beneath SWNT network. The donation of electron to the p-type semiconducting SWNTs increases the electrical resistance.

Regarding the swelling of PMMA of the Pt/PMMA/SWNTs, it could be explained by three possible mechanisms; (I) the swelling of PMMA matrix upon DCM exposure [15,18]. (II) The swelling upon CO_2 produced by dissociation of DCM [33]. The simulation results show that CO_2 could diffuse in PMMA obeying a common hopping mechanism. The origin of solubility of CO_2 in PPMA is due to a stronger gas-polymer interaction, mainly between carbonyl group of polymer and CO_2, resulting in a higher swelling of polymer upon CO_2 uptake. (III) The swelling of PMMA at the interface between Pt NPs and PMMA layer. The swelling of PMMA is enhanced by the presence of inorganic clusters in the polymer with metal content below the percolation threshold [34–39]. After Pt NP decoration, the PMMA retained the same functional groups but its crystallinity degree and thickness decreased. The decrease in the crystallinity degree may enhance the swelling volume of the PMMA upon DCM exposure, resulting in the increase in the response magnitude [40]. Additionally, the morphology of the polymer such as roughness could also effect on the sensor response as reported in the ethanol detection by polypyrrole in which the high surface roughness enhances the sensitivity [41]. Further systematical research into the area of morphology effect of polymer on gas response is necessary.

Fig. 5(d) shows the sensor response of $S_{5,5}$ as a function of DCM concentration in the range of 1700 to 2150 mg/L. A linear relationship was obtained between the sensor response of the Pt/PMMA/SWNT and the concentration of DCM, i.e., the sensor response increased proportionally with DCM concentration. The DCM concentration studied in this research was in a high concentration range. Future work will study the limit of detection of the hybrid Pt/PMMA/SWNT sensor by modifying the sensor measurement system to the ppb-ppm level detection and optimizing the electrode configuration such as the electrode gap. Nevertheless, the advantage of the hybrid Pt/PMMA/SWNT is the significant improvement in response magnitude. The Pt/PMMA/SWNT enabled 69-fold improvement in DCM detection compared to pristine SWNT. Moreover, our proposed sensor can operate under room-temperature condition and consume low power. These advantages let our proposed sensor become a potential candidate for a portable sensing device with real-time monitoring.

4. Conclusion

We successfully demonstrated a DCM sensor with a high response magnitude using the integration of SWNTs, PMMA and Pt NPs. Pt/PMMA/SWNTs exhibited a 69.4-fold improvement in the response to DCM. The sensor response of Pt/PMMA/SWNT linearly increased with increasing DCM concentration. The sensing mechanism of the hybrid sensor was attributed to the incorporation of polymer swelling and catalytic oxidation functions. These results clearly demonstrate that the integration of pristine SWNTs with PMMA and Pt NPs offers a promising material for practical and high-performance DCM sensing applications.

Prime novelty statement

- The novel of our work is the integration of single-walled carbon nanotubes (SWNTs), poly(methyl methacrylate) (PMMA) and platinum nanoparticles (Pt NPs) (hereafter referred to as Pt/PMMA/SWNT) as hybrid materials for dichloromethane (DCM) detection with a high response magnitude.
- The Pt/PMMA/SWNT enabled approximately 69-fold improvement in DCM detection compared to pristine SWNT under room-temperature condition.

Acknowledgments

This work has partially been supported by the National Nanotechnology Center (NANOTEC), NSTDA, Ministry of Science and Technology, Thailand, through its program of Center of Excellence Network. We acknowledge facility support from the Thai Microelectronics Center (TMEC) and the National Metal and Materials Technology Center (MTEC). We also acknowledge the financial support from the Toray Science Foundation (TSF), Japan, the King Prajadhipok and Queen Rambhai Barni Memorial Foundation, and the Thailand Graduate Institute of Science and Technology (TGIST) under contact number 01-55-13.

References

[1] J.N. Armor, Environmental catalysis, Appl. Catal. B Environ. 1 (1992) 221–256, http://dx.doi.org/10.1016/0926-3373(92)80051-Z.

[2] V.H. Vu, J. Belkouch, A. Ould-Dris, B. Taouk, Removal of hazardous chlorinated VOCs over Mn–Cu mixed oxide based catalyst, J. Hazard. Mater. 169 (2009) 758–765, http://dx.doi.org/10.1016/j.jhazmat.2009.04.010.

[3] M.V. Evans, J.C. Caldwell, Evaluation of two different metabolic hypotheses for dichloromethane toxicity using physiologically based pharmacokinetic modeling for in vivo inhalation gas uptake data exposure in female B6C3F1 mice, Toxicol. Appl. Pharmacol. 244 (2010) 280–290, http://dx.doi.org/10.1016/j.taap.2010.01.018.

[4] Q.-Y. Chen, N. Li, M.-F. Luo, J.-Q. Lu, Catalytic oxidation of dichloromethane over Pt/CeO_2–Al_2O_3 catalysts, Appl. Catal. B Environ. 127 (2012) 159–166, http://dx.doi.org/10.1016/j.apcatb.2012.08.020.

[5] S.M. Kanan, O.M. El-Kadri, I.A. Abu-Yousef, M.C. Kanan, Semiconducting metal oxide based sensors for selective gas pollutant detection, Sensors 9 (2009) 8158–8196, http://dx.doi.org/10.3390/s91008158.

[6] G.F. Fine, L.M. Cavanagh, A. Afonja, R. Binions, Metal oxide semi-conductor gas sensors in environmental monitoring, Sensors 10 (2010) 5469–5502, http://dx.doi.org/10.3390/s100605469.

[7] S. Iijima, T. Ichihashi, Single-shell carbon nanotubes of 1-nm diameter, Nature 363 (1993) 603–605, http://dx.doi.org/10.1038/363603a0.

[8] A. Peigney, C. Laurent, E. Flahaut, R.R. Bacsa, A. Rousset, Specific surface area of carbon nanotubes and bundles of carbon nanotubes, Carbon 39 (2001) 507–514, http://dx.doi.org/10.1016/S0008-6223(00)00155-X.

[9] T.W. Odom, Electronic Properties of Single-walled Carbon Nanotubes, 54 (2001) 601–604.

[10] S. Hong, S. Myung, Nanotube electronics: a flexible approach to mobility, Nat. Nanotechnol. 2 (2007) 207–208, http://dx.doi.org/10.1038/nnano.2007.89.

[11] C. Cantalini, L. Valentini, I. Armentano, L. Lozzi, J.M. Kenny, S. Santucci, Sensitivity to NO_2 and cross-sensitivity analysis to NH_3, ethanol and humidity of carbon nanotubes thin film prepared by PECVD, Sensors Actuators B Chem. 95 (2003) 195–202, http://dx.doi.org/10.1016/S0925-4005(03)00418-0.

[12] P. Qi, O. Vermesh, M. Grecu, A. Javey, Q. Wang, H. Dai, S. Peng, K.J. Cho, Toward large arrays of multiplex functionalized carbon nanotube sensors for highly sensitive and selective molecular detection, Nano Lett. 3 (2003) 347–351, http://dx.doi.org/10.1021/n1034010k.

[13] J. Li, Y. Lu, Q.L. Ye, J. Han, M. Meyyappan, Carbon nanotube based chemical sensors for gas and vapor detection, Nano Lett. 3 (2003) 929–933, http://dx.doi.org/10.1021/nl034220x.

[14] W. Wongwiriyapan, S.I. Honda, H. Konishi, T. Mizuta, T. Ikuno, T. Ito, T. Maekawa, K. Suzuki, H. Ishikawa, K. Oura, M. Katayama, Single-walled carbon nanotube thin-film sensor for ultrasensitive gas detection, Jpn. J. Appl. Phys 2 Lett. 44 (2005) http://dx.doi.org/10.1143/JJAP.44.L482.

[15] J.K. Abraham, B. Philip, A. Witchurch, V.K. Varadan, C.C. Reddy, A compact wireless gas sensor using a carbon nanotube/PMMA thin film chemiresistor, Smart Mater. Struct. 13 (2004) 1045–1049, http://dx.doi.org/10.1088/0964-1726/13/5/010.

[16] H. Yoon, J. Xie, J.K. Abraham, V.K. Varadan, P.B. Ruffin, Passive wireless sensors using electrical transition of carbon nanotube junctions in polymer matrix, Smart Materials and Structures. 15 (2006) S14–S20, http://dx.doi.org/10.1088/0964-1726/15/1/004.

[17] M. Castro, B. Kumar, J.F. Feller, Z. Haddi, A. Amari, B. Bouchikhi, Novel e-nose for the discrimination of volatile organic biomarkers with an array of carbon nanotubes (CNT) conductive polymer nanocomposites (CPC) sensors, Sensors Actuators B Chem. 159 (2011) 213–219, http://dx.doi.org/10.1016/j.snb.2011.06.073.

[18] W. Muangrat, T. Chodjarusawad, R. Maolanon, S. Pratontep, S. Porntheeraphat, W. Wongwiriyapan, Poly (methyl methacrylate) and thiophene-coated single-walled carbon nanotubes for volatile organic compound discrimination, Jpn. J. Appl. Phys. 55 (2016) http://dx.doi.org/10.7567/JJAP.55.02BD04 (02BD04 (1–6)).

[19] A. Star, V. Joshi, S. Skarupo, D. Thomas, J.-C.P. Gabriel, Gas sensor array based on metal-decorated carbon nanotubes, J. Phys. Chem. B 110 (2006) 21014–21020, http://dx.doi.org/10.1021/jp064371z.

[20] R. Leghrib, E. Llobet, Quantitative trace analysis of benzene using an array of plasma-treated metal-decorated carbon nanotubes and fuzzy adaptive resonant theory techniques, Anal. Chim. Acta 708 (2011) 19–27, http://dx.doi.org/10.1016/j.aca.2011.09.038.

[21] H. Baccar, A. Thamri, P. Clément, E. Llobet, A. Abdelghani, Pt- and Pd-decorated MWCNTs for vapour and gas detection at room temperature, Beilstein J. Nanotechnol. 6 (2015) 919–927, http://dx.doi.org/10.3762/bjnano.6.95.

[22] J. Jang, S. Kim, K.J. Lee, Fabrication of CdS/PMMA core/shell nanoparticles by dispersion mediated interfacial polymerization, Chem. Commun. 2689–2691 (2007) http://dx.doi.org/10.1039/b703717a.

[23] L. Zhang, F. Li, Y. Chen, X. Wang, Synthesis of transparent ZnO/PMMA nanocomposite films through free-radical copolymerization of asymmetric zinc methacrylate acetate and in-situ thermal decomposition, J. Lumin. 131 (2011) 1701–1706, http://dx.doi.org/10.1016/j.jlumin.2011.03.065.

[24] A. Zanotto, A.S. Luyt, A. Spinella, E. Caponetti, Improvement of interaction in and properties of PMMA-MWNT nanocomposites through microwave assisted acid treatment of MWNT, Eur. Polym. J. 49 (2013) 61–69, http://dx.doi.org/10.1016/j.eurpolymj.2012.10.030.

[25] W. Li, C. Liang, W. Zhou, J. Qiu, Z. Zhou, G. Sun, Q. Xin, Preparation and characterization of multiwalled carbon nanotube-supported platinum for cathode catalysts of direct methanol fuel cells, J. Phys. Chem. B 107 (2003) 6292–6299, http://dx.doi.org/10.1021/jp022505c.

[26] W. Li, M. Waje, Z. Chen, P. Larsen, Y. Yan, Platinum nanopaticles supported on stacked-cup carbon nanofibers as electrocatalysts for proton exchange membrane fuel cell, Carbon 48 (2010) 995–1003, http://dx.doi.org/10.1016/j.carbon.2009.11.017.

[27] A. Jorio, R. Saito, J.H. Hafner, C.M. Lieber, M. Hunter, T. McClure, G. Dresselhaus, M.S. Dresselhaus, Structural (n,m) determination of isolated single-wall carbon nanotubes by resonant Raman scattering, Phys. Rev. Lett. 86 (2001) 1118–1121, http://dx.doi.org/10.1103/PhysRevLett.86.1118.

[28] T. Kim, D. Kwak, Flexible VOC sensors using conductive polymers and porous membranes for application to textiles, Fibers Polym. 13 (2012) 471–474, http://dx.doi.org/10.1007/s12221-012-0471-7.

[29] W. Wongwiriyapan, S. Inoue, T. Ito, R. Shimazaki, T. Maekawa, K. Suzuki, H. Ishikawa, S. Honda, K. Oura, M. Katayama, Highly sensitive detection of carbon monoxide at room temperature using platinum-decorated single-walled carbon nanotubes, Appl. Phys. Express 1 (2008) 1–3, http://dx.doi.org/10.1143/APEX.1.014004.

[30] J.L. Gland, B.A. Sexton, G.B. Fisher, Oxygen interactions with the Pt(111) surface, Surf. Sci. 95 (1980) 587–602, http://dx.doi.org/10.1016/0039-6028(80)90197-1.

[31] D.M. Papenmeier, J.A. Rossin, Catalytic oxidation of dichloromethane, chloroform, and their binary mixtures over a platinum alumina catalyst, Ind. Eng. Chem. Res. 33 (1994) 3094–3103, http://dx.doi.org/10.1021/ie00036a026.

[32] H. Yasumatsu, N. Fukui, Size dependence of low-temperature catalytic activity of CO oxidation driven by platinum clusters directly bound to silicon substrate surface, J. Phys. Chem. C 119 (2015) 11217–11223, http://dx.doi.org/10.1021/jp512172v.

[33] H. Eslami, M. Kesik, H.A. Karimi-Varzaneh, F. Müller-Plathe, Sorption and diffusion of carbon dioxide and nitrogen in poly(methyl methacrylate), J. Chem. Phys. 139 (2013) 124902, http://dx.doi.org/10.1063/1.4821585.

[34] T. Vossmeyer, B. Guse, I. Besnard, R.E. Bauer, K. Müllen, A. Yasuda, Gold nanoparticle/polyphenylene dendrimer composite films : preparation and vapor-sensing properties, Adv. Mater. 14 (2002) 238–242.

[35] A. Convertino, A. Valentini, A. Bassi, N. Cioffi, L. Torsi, E.N.M. Cirillo, Effect of metal clusters on the swelling of gold-fluorocarbon-polymer composite films, Appl. Phys. Lett. 80 (2002) 1565–1567, http://dx.doi.org/10.1063/1.1448858.

[36] S.D. Evans, S.R. Johnson, Y.L. Cheng, T. Shen, Vapour sensing using hybrid organic–inorganic nanostructured materials, J. Mater. Chem. 10 (2000) 183–188, http://dx.doi.org/10.1039/A903951A.

[37] A. Convertino, G. Leo, M. Tamborra, C. Sciancalepore, M. Striccoli, M.L. Curri, A. Agostiano, TiO_2 colloidal nanocrystals functionalization of PMMA: a tailoring of optical properties and chemical adsorption, Sensors Actuators B Chem. 126 (2007) 138–143, http://dx.doi.org/10.1016/j.snb.2006.11.043.

[38] A. Convertino, M. Tamborra, M. Striccoli, G. Leo, A. Agostiano, M.L. Curri, Poly(methyl methacrylate) nanocomposites based on TiO_2 nanocrystals: tailoring material properties towards sensing, Thin Solid Films 519 (2011) 3931–3938, http://dx.doi.org/10.1016/j.tsf.2011.01.359.

[39] N. Cioffi, L. Torsi, I. Farella, D. Altamura, A. Valentini, M. Quinto, L. Sabbatini, P.G. Zambonin, The swelling of vapor-sensitive fluoropolymers modified with metal nanoparticles: interpretation of the material–vapor interaction mechanism, Sensors Actuators B Chem. 100 (2004) 9–16, http://dx.doi.org/10.1016/j.snb.2003.12.058.

[40] S. Lampman (Ed.), Characterization and Failure Analysis of Plastics, ASM International 2003, p. 149.

[41] Q. Fang, D.G. Chetwynd, J.A. Covington, C.-S. Toh, J.W. Gardner, Micro-gas-sensor with conducting polymers, Sensors Actuators B Chem. 84 (2002) 66–71, http://dx.doi.org/10.1016/S0925-4005(01)01076-0.